Applied Mathematics & Information Sciences
An International Journal

http://dx.doi.org/10.18576/amis/110118

An Innovative Method to Estimate Groundwater Level

Wang Iau-Teh[1,2] *and Chung Weihao*[1,*]

[1] Department of Civil Engineering, Chinece Military Academy, Taiwan, R.O.C.
[2] Graduate Institute of Disaster Prevention on Hillslopes and Water Resources Engineering, National Pingtung University of Science and Technology, Taiwan, R.O.C.

Received: 11 Jul. 2016, Revised: 3 Sep. 2016, Accepted: 16 Sep. 2016
Published online: 1 Jan. 2017

Abstract: Soil properties and the position of illegal pumping wells can all be determined through the use of the groundwater level which, however, cannot be measured without the excavation of observation wells or the purchase of ground penetration radar. The former destroys terrain features, and the latter is expensive, aside from its limitations. This paper attempts to solve these problems by estimating groundwater levels economically via atmospheric conditions, and by collecting soil parameters near to the land's surface. Firstly, the Penman-Monteith evaporation formula is explored to deduce the value of the embedded resistance ratio, which governs the involved water content, evaporation speed and, eventually, the groundwater level. Secondly, two theoretical models based on Darcy's law are developed for predicting groundwater levels, one depending on a steady-state assumption and the other being identified as an analytical solution. To justify the first model, the time lapse required before achieving the steady state is estimated by solving numerically the air-liquid two-phase flow equations involving soil temperature variations. For efficiency, a special coordinate transformation is adopted to fix the spatial domains of all related numerical models between 0 and 1. The so-obtained numerical solutions not only testify to the accuracy of the newly developed theoretical models, but they also detect the interactions among air, water, evaporation, and temperature.

Keywords: Groundwater level, Brooks-Corey model, Bowen ratio, surface resistance

1 Introduction

The groundwater level is usually used to estimate other parameters, such as the permeability coefficient, storage coefficient, and the locations of illegal pumping wells. It is affected by atmospheric conditions and the Earth's surface heat flux (such as net solar radiation) at the same time. Based on the atmospheric conditions and the amount of Earth's surface heat flux, the water evaporation rate of the topsoil can be derived from the well-known Penman-Monteith (PM) equation. Nevertheless, it is necessary to know the ratio of surface resistance and aerodynamic resistance [1,2] (g_c^{-1}) in advance. The derived water evaporation rate can then be assumed as the upper-boundary condition in the unsaturated layer water flow simulations, and it is also related to the interactions between the atmosphere and the land, as well as the variations in groundwater levels.

The estimation of groundwater levels has multiple applications, the commonest of which is the derived saturated permeability coefficient of soil which can be calculated from the estimation itself. In recent years, groundwater levels have even been applied to estimate the locations of illegal pumping wells inversely [3]. The defined objective function is the mean square root error of the estimated water level and the mean observed water level. Both the distance between the observation well and the border and the pumping well's location are crucial; otherwise, the drawdown can not be clearly revealed, and this will lead to immense errors in the inverse search. It is also an issue of the density of the observation wells. A method which is low-cost and can effectively estimate the distribution of groundwater levels without excavating observation wells would have a high application value.

Practically, GPR [4,5] (Ground Penetration Radar) is often applied to measure the level of groundwater directly. It can promptly provide information on subterranean topography, foundation depth, and the depth and flow of groundwater, as well as reduce the number of unnecessary monitoring wells. In the GPR method, however, the survey depth in most soils and rocks should not exceed 10 meters. Basically, larger-grained soil, soil with low amounts of expandable clay and dissolved salts

* Corresponding author e-mail: weihao5@yahoo.com.tw

or crystalline bedrock has a higher application value. If the soil has fine grains or more expandable clay, GPR will not be suitable [6] (<1 m). In that case, noise removal and image analysis can become the key to determining whether or not GPR would be successful. Furthermore, the price of GPR is costly, usually between 15,000 USD and 50,000 USD, and it can cost more than 1,000 USD to hire GPR for just one week.

In order to pursue the economic and innovative aspects in practice, this research focused on (i) analyzing the relationship between the resistance ratio g_c^{-1} and the Bowen ratio in the PM model; (ii) establishing the theoretical model of atmosphere-land vapor interaction; (iii) finding a simple and economical non-destructive method (namely, the theoretical solution) to estimate groundwater levels; (iv) verifying the effectiveness of (iii) by applying numerical analyses; and (v) looking into the influence of temperature on moisture content, air pressure, and groundwater levels in unsaturated layers. The results of this research will add support to relevant studies on groundwater levels and, at the same time, make possible a simple and effective replacement method for GPR or observation wells.

2 Deriving of Resistance Ratio g_c^{-1}

With some critical assumptions, the well-known PM model, usually in the form of

$$\lambda E = \frac{\Delta}{\Delta + g_c^{-1}\gamma}(R_n - G) + \frac{\gamma}{\Delta + g_c^{-1}\gamma} B\lambda\,(e_{s2} - e_2), \quad (1)$$

was derived from the following basic formulas:

$$\tau = \rho_a K_m \frac{\partial u}{\partial z}, \quad (2)$$

$$E = -\rho_a K_e \frac{\partial q_v}{\partial z}, \quad (3)$$

$$H = -\rho c_p \mu_T \left.\frac{\partial T}{\partial z}\right|_{z=0}, \quad (4)$$

In above, λ=the latent heat of the evaporating water, E=water evaporation rate, γ=psychrometric constant, $\Delta = de_s/dT$, R_n=net solar radiation, G=heat absorption at the ground, B=variable consisting of atmospheric parameters, e=vapor pressure, e_s=saturated vapor pressure, τ=shear stress, E=evaporation rate, H=sensible heat, u=wind velocity, ρ_a=air density, q_v=specific humidity, c_p=the specific heat of air at a constant pressure, μ_T=heat diffusion coefficient, T=air temperature, g_c^-1= resistance ratio. z is positive upward.K_m and K_e denote momentum and mass diffusion coefficients, respectively. Figure 1 is the definition sketch of our coordinate systems above and below the ground, and the variables often used in this study.

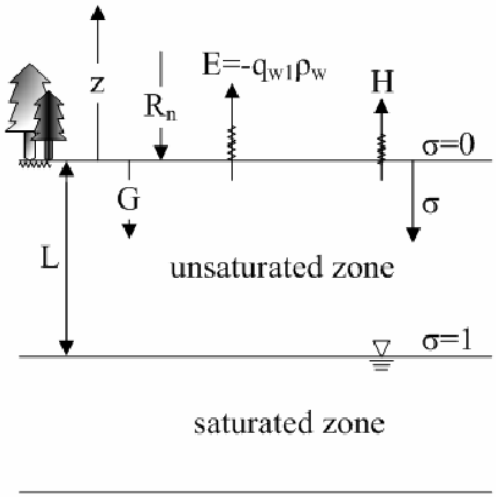

Fig. 1: Definition sketch of the variables involved in this study.

As a key variable in Eq. (1), g_c^{-1}, the resistance ratio of water evaporated from soils (possibly covered with canopy), can be deduced from

$$g_c^{-1} = 1 + \frac{e_0 - e_1}{e_1 - e_2}, \quad (5)$$

based on the mathematic expression of aerodynamic resistance and surface resistance [18]. The subscripts 0, 1, and 2 denote the elevations associated with stomata, leaf surface, and a higher point, respectively. These subscripts will represent topsoil, land surface, and a higher point, respectively, when a soil rather than a canopy is of interest. Since vapor pressure inside the stomata of a leaf (i.e., e_0) is involved, e_0 and e_1 (vapor pressure at leaf surface) must be removed regarding the practicability of Eq. (5). It is worthy now to recall the above mentioned critical assumptions, namely, the equivalent temperature inside or outside a leaf (i.e., $T_0 \approx T_1$) and the saturated water vapor pressure inside the stomata (i.e., $e_0 = e_{0s}$). Accordingly, we have $e_0 = e_{0s} = e_{1s}$ which leads Eq. (5) to be recast as follows:

$$g_c^{-1} = 1 + \frac{e_{1s} - e_1}{e_1 - e_2}, \quad (6)$$

where e_{1s}= the saturated vapor pressure at elevation 1. Supposing H_r, the relative humidity, is given at elevation 1, then $e_1 = H_r e_{1s}$ is fully described by air temperature T_1. Based on Eq. (2) with a logarithmic velocity profile, it can be easily shown that $K_m = \kappa u_* z$ where u_* and κ denote the shear velocity and von-Karman constant, respectively. With the result and $K_e = K_m$ (by Reynolds analogy), Eq. (3) is integrated with respect to z and yields [7]:

$$e_1 = e_2 - \frac{q_{w1}\rho_w p \ln(z_2/z_0)}{0.622\rho_a u_* \kappa}, \quad (7)$$

where z_0=roughness height, p=atmospheric pressure, q_{w1} ($\equiv -E/\rho_w$)= Darcy velocity at the land surface. To relax the differential term in Eq. (4), the following commonly used expression [8] for sensible heat is adopted:

$$H = \kappa u_* \rho c_p \frac{T_1 - T_2}{\ln(z_2/z_1)}, \tag{8}$$

By incorporating Eq. (8) with the definition of the Bowen ratio ($\beta \equiv H/\lambda E$), q_{w1} can be expressed as a function of atmospheric parameters as below:

$$q_{w1} = \frac{-H}{\rho_w \beta \lambda} = \frac{\rho_a c_p \kappa u_*}{\rho_w \beta \lambda \ln(z_2/z_0)} (T_2 - T_1), \tag{9}$$

Substituting Eq. (9) into Eq. (7) yields

$$e_1 = e_2 + \frac{\gamma}{\beta}(T_1 - T_2), \tag{10}$$

where the psychrometric constant $\gamma = c_p p/(0.622\lambda)$. As can be identified, Eq. (10) is a model often employed for estimating the Bowen ratio on site. Finally, e_1 in Eq. (6)can be eliminated by applying Eq. (10), and the result is

$$g_c^{-1} = \frac{\beta}{\gamma}\left(\frac{e_{1s} - e_2}{T_1 - T_2}\right), \tag{11}$$

Eq. (11)establishes a link between β and ${g_c}^{-1}$, and provides us with another way to compute ${g_c}^{-1}$ values, once β and e_{1s} are measured. For simplicity, we focus on Eq. (6) with the relative humidity a known variable. For other related essays, please refer to the work of Lakshmi and Wood [9] and Allen *et al.* [1,2]. At this point, on the basis of Eq. (8) and the definition of β, the water evaporation rate of topsoil can be represented in the function of β as:

$$E = \frac{\kappa u_* \rho c_p}{\lambda \beta} \frac{T_1 - T_2}{\ln(z_2/z_0)}, \tag{12}$$

In practice, β is usually obtained from Eq. (10). Since g_c^{-1} has been excluded from Eq. (12), the E values can be easily obtained, without needing to measure the surface resistance, net solar radiation, and heat absorption on the surface of the ground. It is therefore simpler and more economical compared to the PM model. The E value computed by the PM model with Eq. (6) or by Eq. (12) with Eq. (10) is a vital parameter when estimating the groundwater level for a quasi-steady state flow condition, as will be introduced below.

3 Theoretical Models of the Groundwater Level

Along with the determination of g_c^{-1}, β, and E, this section pursues the theoretical solutions to estimate groundwater level. When groundwater level L changes, the unsaturated zone expands or shrinks as a consequence. This provokes the problem of moving boundary and imposes an obstruction on numerical analyses. In response, this paper sets $\sigma = z/L$ to fix the unsaturated zone such that $\sigma \in [0,1]$. As for time, the symbol t may be retained since no temporal transformation is performed.

Fluid velocity in topsoil can be expressed as follows [10] according to the Darcy's law:

$$q_{w1} = \left[K_w\left(1 + \frac{1}{L}\frac{\partial \psi}{\partial \sigma} - \frac{1}{L}\frac{\partial h_a}{\partial \sigma}\right)\right]_{\sigma=0}, \tag{13}$$

where K_w=soil conductivity, L=groundwater level measured from the ground, ψ=suction head, h_a=air pressure head. When the topsoil is covered by impermeable layers such as tar or plastic sheets, E=0, which means q_{w1}=0. After a certain period of time, if the distribution of the moisture content reaches the steady state, Eq. (13) can be applied to all the depths. Therefore, by integrating Eq. (13) with respect to σ and using the Brooks-Corey equation [11]:

$$\Theta = \frac{\theta_w - \theta_{wr}}{\theta_{ws} - \theta_{wr}} = \left(\frac{\psi_b}{\psi}\right)^{\eta}, \tag{14}$$

we have

$$(1-\sigma)L = \psi_b\left(\Theta^{\frac{-1}{\eta}} - 1\right) + h_{aL} - h_a, \tag{15}$$

where Θ=effective saturation, θ_w=water content, ψ_b=the bubbling pressure head, h_{aL}=air pressure head at $\sigma = 1$, and η= the Brooks-Corey parameter. Now, assuming the air pressure head is not to change as the depth varies (i.e. there is no air flow in the soil.), Eq. (15) gives

$$L = \psi_b(\Theta_1^{-1/\eta} - 1), \tag{16}$$

where Θ_1= effective saturation of the ground. This solution may be regarded as the initial condition of soil water content for latter numerical simulations. Surprisingly enough, we find that Eq. (16) is valid for all types of soil and only depends on the properties of the specific surface soil. When $E \neq 0$, both $q_{w1}$and $K_w$in Eq. (13) are not negligible. This research employs the Burdine's model [19] so that $K_w = K_s\Theta^{3+\frac{2}{\eta}}$ in which K_s denotes the conductivity when the soil is saturated with water. It then can be validated according to Eq. (14) and the identity of Eqs. (9) (13) that

$$\frac{\psi_b}{\eta L}\Theta^{2+\frac{1}{\eta}}\frac{\partial \Theta}{\partial \sigma} - \varphi\Theta^{3+\frac{2}{\eta}} = \Im, \tag{17}$$

where $\varphi = 1 - \partial h_a/\partial z$ and $\Im = H/(\beta\lambda\rho_w K_s) = E/(\rho_w K_s)$. If the unsaturated zone flow remains quasi-steady state, that is, q_{w1} (or E) changes in an infinitely small frequency, $\Im$ becomes almost a constant and invariant with soil depth. In this

case, Eq. (17) will be applicable to the entire unsaturated zone instead of the land surface only. By introducing the boundary conditions that $\Theta = \Theta_1$ at $\sigma = 0$ and $\Theta = 1$ at $\sigma = 1$, the groundwater level is solved from Eq. (17) using the method of separation of variables:

$$L = \frac{\psi_b}{\eta} \int_{\Theta_1}^{1} \frac{\Theta^{2+\frac{1}{\eta}}}{\Im + \varphi\Theta^{3+\frac{2}{\eta}}} \partial\Theta, \tag{18}$$

The L value can be computed by numerical integration if φ, $\Im$, and the vertical distribution of $\Theta$is known as a *priori*. When $\Im > 0$ (i.e., $E > 0$) and $\varphi \to 1$, the above integration can be obtained and Eq. (18) becomes

$$L = \psi_b \xi \left(\frac{1}{\Im}\right)^{\xi} [\beta_I(\varsigma_4, \delta, \xi)\beta_c(\delta, \xi) - \beta_I(\varsigma_3, \delta, \xi)\beta_c(\delta, \xi)], \tag{19}$$

after a lengthy derivation [10], where $\xi = 1/(3\eta + 2)$, $\delta = 1 - \xi$, $\varsigma_1 = 1 + \Im$, $\varsigma_2 = 1 + \Im\Theta_1^{-3-2\eta^{-1}}$, $\varsigma_3 = 1/\varsigma_2$, $\varsigma_4 = 1/\varsigma_1$. β_c and β_I represent the complete and incomplete beta functions, respectively. Therefore, L only depends on ψ_b and three other dimensionless variables which are η,$\Im$, and Θ_1. It becomes apparent that sampling soils from the land surface is sufficient for estimating L by the presently developed theory, as long as the unsaturated zone is homogeneous. Water contents of the deeper soil are irrelevant with the estimation of L. Eqs. (16) and (19) are the solutions under (quasi-)steady-state conditions. Nevertheless, E, or the water flow in unsaturated layers in a single day, tends to be unstable because the net solar radiation is not fixed. Therefore, as mentioned previously, when applying these two equations practically, it is recommended that an insulation panel or impermeable pavement (making E=0) be put in place to segregate the heat and vapor interaction between the atmosphere and the land in order to achieve the goal of reaching the forced steady state. Even if it is time consuming to reach the steady state (as will be discussed), g_c^{-1} can be tested first according to Eq. (6) . Then, the value of E can be derived based on Eq. (12) or the PM model as the upper-boundary condition of the water flow in the unsaturated zone. Afterwards, the levels of groundwater can be derived by the analytical solutions. A carefully designed numerical experiment will verify the authenticity of Eqs. (16) and (18), and Eq. (19) at the same time.

4 Numerical Model of the Two-Phase Flow

In addition to estimating the consumed time for reaching the forced steady state, this research at the same time looks into the influence of the heat flux on groundwater levels, behaviors of the gas flow in the soil, as well as the effect of soil temperatures on the gas–liquid two-phase flow by carrying out numerical experiments. The control equations applied include the heat conduction equation of soil [12], water pressure head and air pressure head equations of the soil [13], ideal gas equation, and one-dimensional control equations of the groundwater [14], as shown below, respectively:

$$\frac{\partial T_s}{\partial t} = \frac{\partial}{\partial z}\left(D_T \frac{\partial T_s}{\partial z}\right), \tag{20}$$

$$q_w = -\frac{kk_{rw}}{\mu_w}\left(\frac{\partial P_w}{\partial z} - \rho_w g\right), \tag{21}$$

$$q_a = -\frac{kk_{ra}}{\mu_a}\left(\frac{\partial P_a}{\partial z} - \rho_a g\right), \tag{22}$$

$$\rho_a = \frac{P_{a0} + h_a\rho_w g}{R_a T}, \tag{23}$$

$$S_y \frac{\partial L}{\partial t} + q_L = J, \tag{24}$$

In above, T_s= soil temperature, D_T= thermal diffusion coefficient, ρ_w= water density, q_w = the Darcy's velocity of water, q_a= the Darcy's velocity of air, q_L= the Darcy's velocity of water just above the groundwater level, k = intrinsic permeability, k_{rw}= the relative permeability of water, ρ_a= air density, P_w= water pressure, P_a= air pressure, g= gravity acceleration, R_a= ideal gas constant, P_{a0}= initial air pressure in soils, S_y= aquifer storage coefficient, L= groundwater level, J= horizontal groundwater flow including source or sink.

To solve Eqs. (21) and (22) for water and air pressure heads, we define a fluid pressure head as $h_j = (P_j - P_{a0})/\rho_w g$ and transform the both equations into the following forms, respectively, after a lengthy algebra [15,16]:

$$C_w \frac{\partial h_w}{\partial t} = \left(\frac{\partial K_w}{\partial z} + \frac{\partial K_w}{\partial \psi}\right)\frac{\partial h_w}{\partial z} + K_w \frac{\partial^2 h_w}{\partial z^2} + C_w \frac{\partial h_a}{\partial t} - \frac{\partial K_w}{\partial \psi}\frac{\partial h_a}{\partial z}, \tag{25}$$

$$\Omega \frac{\partial h_a}{\partial t} = \left(\frac{\partial \rho_a K_a}{\partial z}\right)\frac{\partial h_a}{\partial z} + \rho_a K_a \frac{\partial^2 h_a}{\partial z^2} + \rho_a C_w \frac{\partial h_w}{\partial t} - \frac{1}{\rho_w}\frac{\partial \rho_a^2 K_a}{\partial z} + \frac{\theta_a P_a}{R_a T^2}\frac{\partial T}{\partial t}, \tag{26}$$

where $C_w = -\partial\theta_w/\partial\psi$, $\Omega = \theta_a\rho_w g/(R_a T) + \rho_a C_w$ with K_w and K_a being the relative conductivity for water and air, respectively. As for the determination of D_T (in SI units), the following modified model of De Vries [3] is adopted:

$$D_T = \frac{10^{-6} k_T}{1.94\theta_m + 2.50\theta_c + 4.19\theta_w}, \tag{27}$$

where k_T is the heat conduction coefficient of soil and θ_m and θ_c the fractions of minerals and organic matters,

respectively. The lateral groundwater flow rate J is neglected in this study regarding the one-dimensional unsaturated zone flow.

By calculating these five simultaneous equations, the variations with time and space of soil temperature T_s, air pressure head h_a, water pressure head h_w, air density ρ_a, and groundwater level L can be derived. Auxiliary equations, meanwhile, include the Brooks-Corey model and the internal permeability coefficient model. In order to be more accurate, this research also applies regression analysis to make hydraulic conductivity the function of temperature. This measure fortifies what researches [17, 15] have lacked. Some data in textbooks [17] have been used as reference for the soil characteristic parameters, such as suction head ψ.

Due to the fact that the groundwater level varies with time in the numerical simulations, this research fixes the simulated space by using again the coordinate conversion $\sigma = z/L$ to reach the solution more easily. The controlling equation after coordinate conversion is discretized by the finite difference method. First-order accuracy is introduced with regard to time, while second-order accuracy is applied concerning space. Also, the difference equation has been presented explicitly to enhance the efficiency of iteration. The results of numerical experiments provide Eqs. (16) (18) (19) with the data used to estimate L.

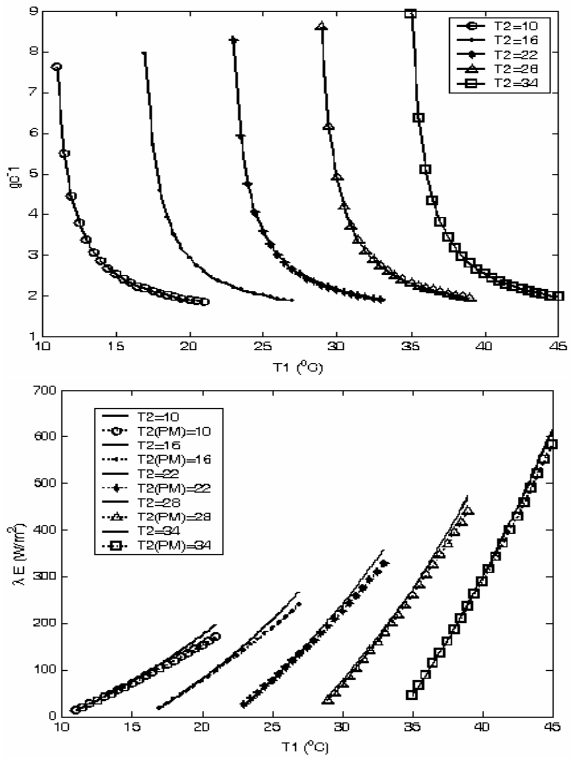

Fig. 2: Curves of g_c^{-1} (up sub-figure) and λE (down sub-figure) that vary with T_1 for different values of T_2.

5 Results

The silt loam was set as an example to perform the numerical simulation. There were in total 101 mesh grids. The time interval Δt was 1200 seconds; the initial groundwater level was set to be 3.6 meters under the ground's surface; the wind speed was u = 2 m/s; and the storage coefficient was S_y=0.1θ_{ws}. The property parameters of the silt loam were as follows: θ_{ws}= 0.501, θ_{wr}= 0.015, $|\psi_b|$= 207.6mm, and K_s = 6.8mm/hr. The fractions of minerals and organic matters were $\theta_m = (1-\theta_{ws})/2$ and $\theta_c = \theta_m$, respectively. Underground water temperature was $T_g = 20^0C$. For a better convergence rate, 100 warm-up mathematical calculations were done before the formal simulation, including the iteration.

In order to study the time consumed to reach the forced steady state when E=0 after the topsoil was covered by airtight plastic sheets, the E value was assumed to match the existing Gaussian distribution at first, then increase slowly. After the E value reached the maximum, it then decayed to zero immediately. That is to say, when $0 < t < 12$, $\lambda E = c_1 \exp\left[-(t-12)^2/c_2^2\right]$, or E=0.

Then again, for the purpose of researching the influence of topsoil temperatureT_1on the distribution of Θ, G (ground surface heat absorption), and h_a(soil gas pressure), there were two different scenarios in the numerical simulation, i.e., with T_1 assumed separately as 25^0C and 45^0C according to Eq. (12). The corresponding c_1s was set to be 30 W/s and 60 W/s, respectively. Also, $c_2 = 4.456$ hours. Figs. 3 to 6 indicate the corresponding results of the calculations. Their up and down sub-figures correspond to the above mentioned first and second conditions, respectively.

Fig. 2 shows the curves of g_c^{-1} (up sub-figure) and λE (down sub-figure) that vary with land surface temperature T_1 for different values of air temperature T_2. Relative humidity is assumed as 70% and invariant with height. The up sub-figure reveals that g_c^{-1} commonly falls within the range $1 < g_c^{-1} < 10$, quite close to those deduced from Lakshmi and Wood [9] and Allen *et al.* [1,2]. The solid lines in the down sub-figure show the results of Eq. (12). Since error is small and the variation trend of each line agrees fairly well with that according to the PM model, the validity of Eqs. (11) and (12) is assured.

Figs. 3 and 4 represent, respectively, the curves showing the variations of Θ and $h_a$of the soil with time. As revealed in Fig. 3, when the abscissa was around 12, the curve at the bottom showed a small slump (corresponding to the change of E). This indicated that the unsteady state of Θ was limited in the shallow soil, and that the E value increased as Θ declined. That is to say, the soil dried as the sunshine increased, which was quite realistic. Then again, as shown in the diagram, the

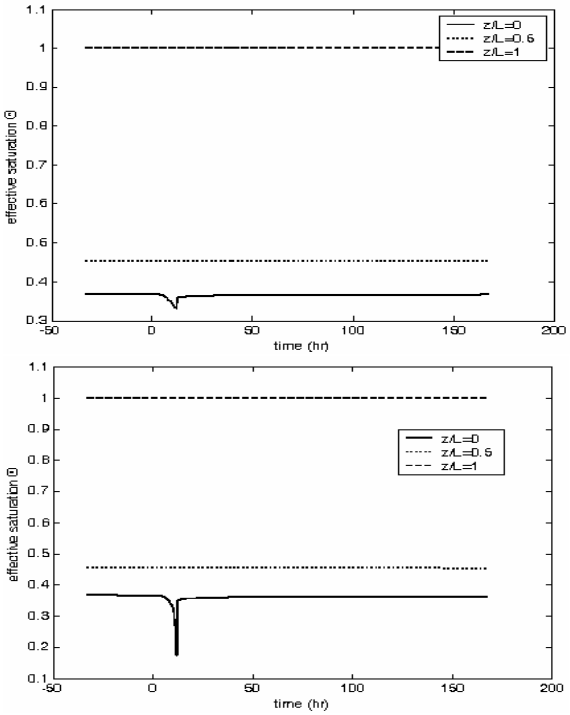

Fig. 3: Curves showing the effective saturation Θ at different depths with the changes in time.

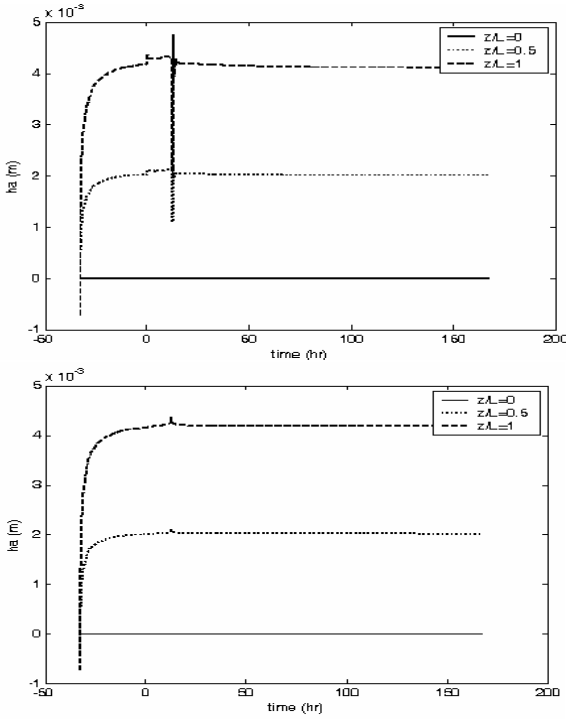

Fig. 4: Curves showing the air pressure head h_a at different depths with the changes in time.

deeper slump on the down-hand side than on the up-hand side showed that the increase of E or T_1 triggered major decreases in the moisture content of the ground surface. It was observed that, as shown in Fig. 4, h_a rose as the depth increased and had a corresponding fluctuation as the E value varied. This fluctuation is evident in the diagrams on both sides, indicating that the variation of E or T_1 affected h_a.

In Fig. 5, the heat absorption G were computed according to $G \equiv -k_T \left.\frac{\partial T_s}{\partial z}\right|_{z\to 0}$. Corresponding to the first and second conditions, respectively, the maximum G values were 37 and 185 W/m^2, and the minimum G values approached to 4 and 16 W/m^2. All the values were far smaller than 600W/m ^{2} ($\approx$ the reasonable value of net solar radiation in summer), which showed that the calculation results were within the reasonable range. This figure also showed the rationality that the G value grew as E or T_1 increased. Furthermore, under the condition of $T_1 < 60^0C$, it could be also observed that the heat conducting distance of the soil was extremely limited. The calculated temperature variation of the topsoil rarely reached soil deeper than 2 m, which reflected the reality.

Fig. 6 shows a comparison between the numerical solution and the theoretical solutions. Clearly, the two theoretical solution curves representing Eqs. (18) and (19) showed almost the same fluctuation, whether in the period of warm-up calculations or under formal

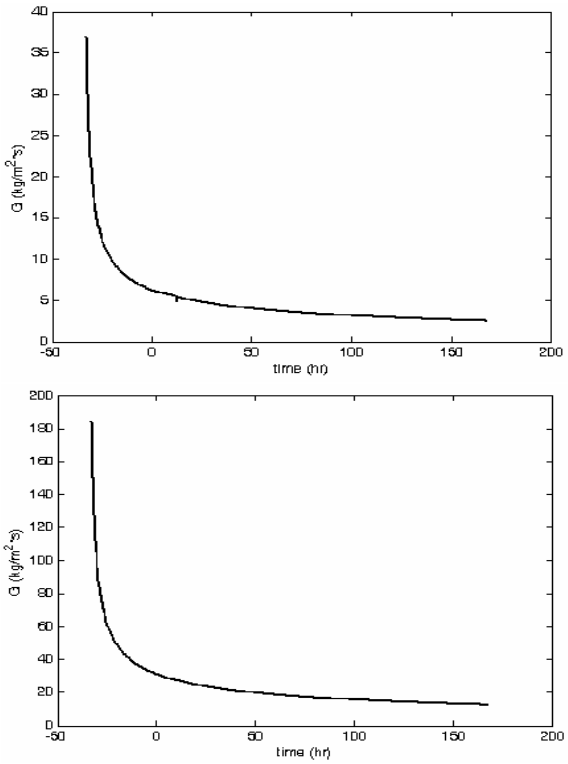

Fig. 5: Curves showing the heat absorption by a silt-loam with the changes in time

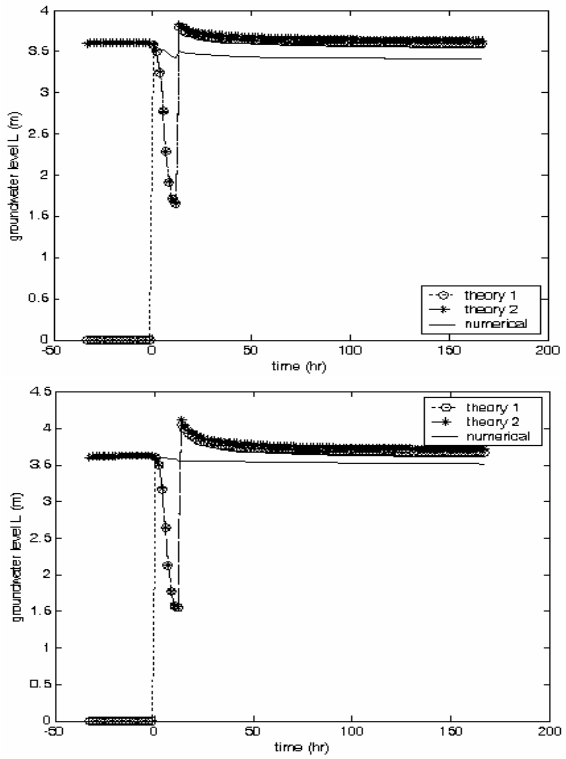

Fig. 6: Curves showing the change of groundwater level L with time (The solid lines represent the numerical solutions. The stars and circles connected by dotted lines indicate, respectively, the theoretical solutions of Eqs. (18) and (19). The dotted stars and dotted circles almost overlap when the abscissas were greater than 0.)

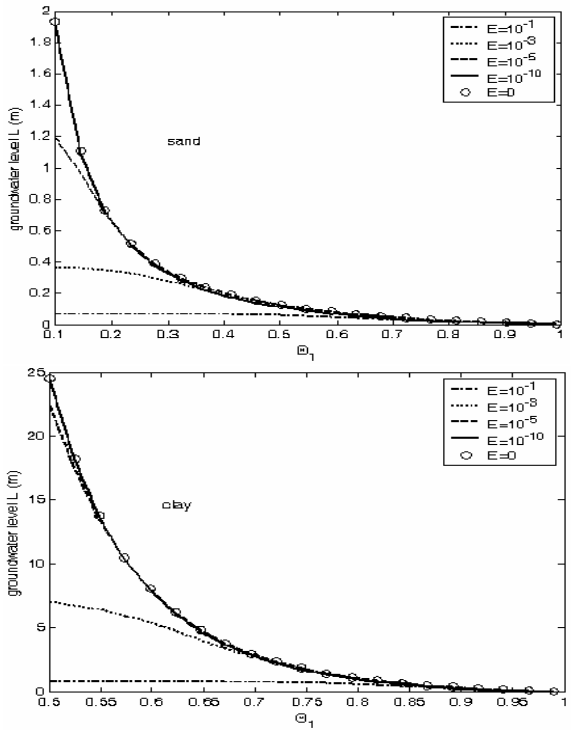

Fig. 7: The variation curves of L with Θ_1 for different E values. (up: sand, down: clay)

simulations (i.e., when the abscissa was greater than 0). This showed that Eq. (18) was capable of replacing the more complicated Eq. (19), even if it was simpler. Moreover, the theoretical solution curves were higher than the solid lines of the numerical simulations regardless of which ones they were. Hence, Eqs. (18) and (19) could have overestimated the levels of ground water, but the error was acceptable. The result validated not only the theoretical solutions but also the numerical experiment itself. Moreover, the solid line reached the steady state approximately 24 hours ($63\Delta t$) after the initiation of the unsteady simulation, and provided the timing of applying Eqs. (18) and (19) . In this figure, it can also be observed that the L value of the diagram on the up-hand side is lower than that on the down-hand side under the steady state. That is, the L value increased as the E value rose. More attention should be paid to the fact that the L value only changed marginally even when the E value doubled.

Due to the fact that Eqs. (16) and (18), and (19) were theoretical solutions with the premise of steady state, storage coefficient S_y was excluded from them both. In the numerical experiments, multiple calculations showed that L reduced as S_y increased, but S_y had no great influence on L. Based on the existing data, when S_y increased from $0.001\theta_{ws}$ to $0.1\theta_{ws}$, the numerical solutions of L approached 3.6 m and 4.0 m, respectively, while the theoretical solutions were both approximately 4.0 m. Therefore, the error between theoretical and numerical solutions did not exceed 0.5 m even if the S_y value was very small.

Figure 7 showed the variation of groundwater level L with the effective land surface saturation Θ_1. The groundwater level was computed by Eqs. (16) and (19), and two soil classes, sand and clay, were chosen for solution comparisons. Property parameters of each soil were $\eta = 0.694$ and $\psi_b = 0.0726$m for sand, and $\eta = 0.165$ and $\psi_b = 0.373$m for clay [18]. As observed from both subfigures, L decreased with the increasing E for a fixed Θ_1 value, which was consistent to the real situation. It was also seen that L increased rapidly when Θ_1 became smaller if E approached to zero. The curves then passed through all the empty circles that represented Eq. (16), thus validating Eq. (19) again. This figure showed that the groundwater table (not level) in a sandy unsaturated zone was usually much shallower than that in other unsaturated zones if the same E and Θ_1 was retained. Eq. (16) would be a good substitution for Eq. (19) only when the ground is quite wet.

6 Conclusions

This research discovered that Eqs. (16) and (19) were both economically and practically viable, and could be used to estimate the levels of groundwater effectively. Their application timing was 24 hours after the ground surface was covered by airtight plastic sheets. Under this condition, Eq. (16) could be adopted to replace Eq. (19) and not restricted by soil types if the ground was almost saturated. According to the two equations, L depended on ψ_b and three other dimensionless variables, η,$\Im$, and Θ_1. Eq. (18) was applicable when the vertical distribution of Θ was available. If the outcome of the numerical experiments was set as the benchmark, the error of Eqs. (18) and (19) would be within 10 centimeters.

The E value exerted evident influence on Θ and G. It also has a great impact on L for a dry soil. If g_c^{-1} remained constant, the E value often increased as $T_1 - T_2$ (or T_1) increased. By numerical experiments, Θ showed no obvious variation when h_a was taken into consideration. The single-phase flow, therefore, was likely able to substitute for the two-phase flow. The integration of Eqs. (6) (10) (12) is the optimal substitution for the PM model, making the E values appeared in Eq. (19) obtainable accordingly. To explore the interactions among air, water, evaporation, and temperature, Eqs. (9) and (19) are useful.

Acknowledgement

This work was sponsored by research grant NSC 99-2221-E-145-005 from the National Science Council of Taiwan. The generous fellowships in CMA provided valuable support and guidance on the research for which I am grateful.

References

[1] R.G. Allen, L.S. Pereira, D. Raes and M. Smith, Crop evapotranspiration, Guidelines for computer crop water requirements, Irrigation and Drainage, Food and Agricultural Organization of the United Nations (FAO), Rome, Italy, (1998), 56.

[2] R.G. Allen, L.S. Pereira, M. Smith, D. Raes and J. L. Wright, FAO-56 dual crop coefficient method for estimating evaporation from soil and application extensions. *Journal of Irrigation and Drainage Engineering*, ASCE. Vol.131, No.1, (2005b), 2-13.

[3] S.T. Lin, C.H. Chen, Y.C. Tan, S.C. Chen and K.Y. Ke, Investigation of Identifying the Place of Illegal Discharge Well with Tabu Search Method Cooperated with Adjoint State Method. *Journal of Taiwan Water Conservancy*. Vol.57, No.2, (2009), 1-11.

[4] S.F. Shih and J.A. Doolittle, Using radar to investigate organic thickness in the Florida everglades. *Soil Science Society of America Journal*. Vol.48, No.3, (1984), 651-656.

[5] G.C. Topp, J.L. Davis and A.P. Anan, Electro-magnetic determination of soil water content?G measurement in coaxial transmission lines. *Water Resources Res.*, Vol.16, (1980), 574-586.

[6] J.S. Mellett, Location of human remains with ground-penetration radar. *Geological Survey of Finland*. Special Paper Vol.16, (1992), 359-365.

[7] W.H. Chung and I.T. Wang, On the application of air-liquid two phase flow in the theoretical estimation of groundwater level, Proposal of National Science Council, NSC 99-2221-E-145-005, Taiwan, 2010.

[8] J.M. Wallace and P.V. Hobbs, Atmospheric Science-An Introduction Survey, Academic Press, New York, 1995.

[9] V. Lakshmi and E.F. Wood, Diurnal cycles of evaporation using a two-layer hydrological model. *Journal of Hydrology*. Vol.204, (1998), 37-51.

[10] W.H. Chung and Y.I. Kang, Assessing the adequacy of static models applied to bare soil evaporation in view of the trivial diurnal variation of surface soil moisture. *Journal of the Chinese Institute of Civil and Hydraulic Engineering*, Vol.17, No.4, (2005), 587-602.

[11] R.H. Brooks and A.T. Corey, Properties of porous media affecting fluid flow. *Jour. Irrig. Drain. Div., Proc.* ASCE, Vol.92(IR2), (1966), 62-88..

[12] D.A. De Vries, Thermal properties of soils, 210-235, Ch. 7 in Van Wijk, W. R. (Ed.), "Physics of plant environment, North-Holland Pub. Co., Amsterdam, 382 (1963).

[13] P.J. Binning, Modeling unsaturated zone flow and contaminant transport in the air and water phases, Ph.D. dissertation, Dept. of Civil Eng. & Operations Res., Princeton University, U.S. A., 1994.

[14] J. Bear, Hydraulics of groundwater, McGraw-Hill Book Co., New York, 1979.

[15] W.H Chung and Y.H. Hu, Interaction of heat transfer and air-liquid dual phase flows during the evaporation process for bare soils. *Journal of Taiwan Water Conservancy*. Vol.57, No.2, (2009), 1-15.

[16] F.C. Tao?AAn Application of Finite Analytic Method in Unsaturated zone?AMaster dissertation, Department of Civil Engineering, National Taiwan University, Taiwan, 1995.

[17] G.J. Weir and W.M. Kissling, The influence of airflow on the vertical infiltration of water into soil. *Water Resources Res.*, Vol.28, No.10, (1992), 2765-2772.

[18] J.A. Smith, class notes, CIV 583, Department of Civil Engineering & Operations Research, Princeton University, NJ., U.S.A.

[19] N.T. Burdine, Relative permeability calculation from size distribution data, trans. Am. Inst. Min. Metall. Pet. Eng. 198, (1953), 71-78.

Wang Iau-Teh received his Master's degree from Chung-Cheng Institute of Technology, Taiwan, R.O.C. in 2004, is presently a postgraduate student in Ph.D. degree at Graduate Institute of Disaster Prevention on Hillslopes and Water Resources Engineering, National Pingtung University of Science and Technology. Being a lecturer in the Department of Civil Engineering, Chinese Military Academy. Taiwan, R.O.C., he has been working on slope stability problems, applications of GIS, underground engineering, etc..

Chung Weihao received his Ph.D. degree from Princeton University, is a professor of the Department of Civil Engineering, Chinese Military Academy, Taiwan, R.O.C.. Also, he has been teaching at the Department of Marine Environment, National Sun Yat-sen University for over ten years. Professor Chung specializes in physical hydrology, water resources engineering, and fluid dynamics.